https://doi.org/10.5194/gmd-2024-4
Preprint. Discussion started: 21 February 2024

Geoscientific Model Development Discussions

Southern Ocean Ice Prediction System version 1.0 (SOIPS v1.0): description of the system and evaluation of synoptic-scale sea ice forecasts

Fu Zhao[1], Xi Liang[1], Zhongxiang Tian[1], Ming Li[1], Na Liu[1], Chengyan Liu[2]

[1]Key Laboratory of Marine Hazards Forecasting, National Marine Environmental Forecasting Center, Ministry of Natural Resources, Beijing, China.
[2]Southern Marine Science and Engineering Guangdong Laboratory (Zhuhai), China.

Correspondence to: Xi Liang (liangx@nmefc.cn)

Abstract. An operational synoptic-scale sea ice forecasting system for the Southern Ocean, namely Southern Ocean Ice Prediction System (SOIPS), has been developed to support ship navigation in the Antarctic sea ice zone. Practical application of the SOIPS forecasts had been implemented for the 38th Chinese National Antarctic Research Expedition for the first time. The SOIPS is configured on an Antarctic regional sea-ice–ocean–ice-shelf coupled model and an ensemble-based Localized Error Subspace Transform Kalman Filter data assimilation model. Daily near-real-time satellite sea ice concentration observations are assimilated into the SOIPS to update sea ice concentration and thickness in the 12 ensemble members of model state. By evaluating the SOIPS performance on forecasting sea ice metrics in a complete melt-freeze cycle from October 1, 2021 to September 30, 2022, this study shows that the SOIPS can provide reliable Antarctic sea ice forecasts. In comparison with the OSISAF data, annual mean root mean square errors of the sea ice concentration forecasts at leading time of up to 168-hour are lower than 0.19, and the integrated ice-edge errors of sea ice forecasts in most freezing months at leading times of 24-hour and 72-hour maintain around 0.5×10^6 km^2 and below 1.0×10^6 km^2, respectively. With respect to the scarce ICESat-2 observations, the mean absolute errors of the sea ice thickness forecasts at leading time of 24-hour are lower than 0.3 m, which is in range of the ICESat-2 uncertainties. Specifically, the SOIPS has a promised capacity in forecasting sea ice drift, both in magnitude and direction. The derived sea ice convergence rate forecasts have a high potential in supporting ship navigation on local fine scale.

1 Introduction

Surrounding the Antarctica, sea ice motion in the Southern Ocean is fast. This situation is partly caused by the natural feature of Antarctic sea ice with thin first-year ice dominating the majority. Wind force leads to faster ice speed if ice thickness is thinner. Moreover, the severe Antarctic environmental conditions, such as frequent westerly cyclones, complicated surface ocean circulation system, drastic nighttime katabatic winds off the ice-shelf, also promote the rapid ice motion. Beyond the Antarctic Peninsula, the topographic shape of high-latitude Southern Ocean without a land barrier in the zonal direction provides an advantage for rapid sea ice movement (Worby et al., 1998; Heil and Allison, 1999; Turner et al., 2002; Wang et al., 2014; Womack et al., 2022). Energetic sea ice in the Southern Ocean has become one of the major challenges to safety

https://doi.org/10.5194/gmd-2024-4
Preprint. Discussion started: 21 February 2024


Geoscientific Model Development Discussions

maritime navigation due to the lack of timely and accurate sea ice forecasting information (Wagner et al., 2020), e.g. during austral summer of 2013/2014 both the Russian icebreaker *MV Akademik Shokalskiy* and the Chinese icebreaker *MV Xue Long* were trapped in the Adélie Depression region by quickly convergent sea ice under the influence of several cyclones (Witze, 2014; Turney, 2014; Zhai et al., 2015). Earlier in November 2007, a cruise ship *MS Explorer* sunk between the South Shetlands and Grahams Land in the Bransfield Strait, after striking an iceberg near the South Shetland Islands, an area which is usually stormy but was calm at the time. Hence, reliable synoptic Antarctic sea ice forecasts are of great important to the Antarctic maritime commercial and scientific activities in the coming decades, when the human activities in the Southern Ocean are expected to be prosperous.

However, partly owing to the relative small amount of customers who needs Antarctic sea ice information, few attempts have been made by international weather forecasting centers to construct operational synoptic sea ice forecasting system for the Southern Ocean, in comparison to the multiple kinds of Arctic sea ice forecasting systems. The Canadian Meteorological Center (CMC) operates the Global Sea Ice Ocean Forecast System (GIOPS; Smith et al., 2016) which is built on the Nucleus for European Modelling of the Ocean (NEMO) version 3.1 and the Los Alamos National Laboratory Community Ice CodE (CICE) version 4.0, and the system is driven by atmospheric forcing from the Global Deterministic Prediction System. Since 2011, the GIOPS provides 10-day forecasts of global ocean and sea ice including the Southern Ocean at a resolution of 0.25°. The United Kingdom Met Office (UKMO) operates the Forecast Ocean Assimilation Model (FOAM; Blockley et al., 2014) which is also based on the NEMO and the CICE. Driven by atmospheric variables at ocean surface from the Met Office Unified Model (UM) global Numerical Weather Prediction (NWP) system, the FOAM produces 7-day forecasts of global ocean tracers, ocean currents and polar sea ice with a horizontal resolution of 0.25°. Under the framework of Copernicus Marine Environment Monitoring Service (CMEMS), the Mercator Ocean has developed a global ocean real-time monitoring and 1/12° high-resolution forecasting system (GLO-HR; Lellouche et al., 2018) based on the NEMO model and the Louvain-la-Neuve Sea Ice Model version 2 (LIM2), and the atmospheric forcing is taken from the Integrated Forecast System (IFS). The GLO-HR delivers 10-day forecasts for global ocean and polar sea ice on a daily basis. The US Navy's Global Ocean Forecast System version 3.1 (GOFS 3.1) is based on the HYbrid Coordinate Ocean Model (HYCOM) and the CICE, and provides a global sea ice prediction capability including both the Arctic and the Antarctic (Posey et al., 2015). SEAS5, the fifth generation seasonal forecast system of the European Centre for Medium-Range Weather Forecasts (ECMWF), which is constituted by the NEMO ocean model, LIM2 sea ice model and IFS atmospheric model, has a horizontal resolution of 0.25° for global ocean and sea ice and provides 10-day forecasts of Antarctic sea ice cover and snow depth (Johnson et al., 2019). Nevertheless, all the above-mentioned operational forecasting systems are built on global coupled models, and their focus is not purely on Antarctic sea ice forecasts. Although resolution of global models is constantly becoming finer, regional ice-ocean coupled models normally with higher resolution and lower computational cost still offer significant advantages when appropriate initial and boundary conditions are adopted (Mu et al., 2019; Liang et al., 2020; Ren et al., 2021).

https://doi.org/10.5194/gmd-2024-4
Preprint. Discussion started: 21 February 2024


Geoscientific Model Development Discussions

Data assimilation is an essential way to reduce short-term forecast uncertainties by providing an optimal estimated initial state, and various data assimilation algorithms have been widely used to assimilate multi-source observations into the sea ice forecasting and analysis systems (Lindsay and Zhang, 2006; Massonnet et al., 2013; Luo et al., 2021). Both the GIOPS and GLO-HR use System Assimilation Mercator version 2 (SAM2) as their ocean assimilation systems, which was developed from the Singular Evolutive Extended Kalman (SEEK) algorithm (Tranchant et al., 2006). The FOAM and SEAS5 adopt 3D-Var data assimilation systems for use with NEMO, namely NEMOVAR (Mignac et al., 2022; Mogensen et al., 2009, 2012). The GOFS 3.1 employs the Navy Coupled Ocean Data Assimilation (NCODA) system based on 3D-Var method (Cummings and Smedstad, 2014). These systems mainly assimilate near-real-time satellite observations of sea ice concentration, sea level anomaly, sea surface temperature together with in situ observations of ocean temperature and salinity profiles. Previous studies have shown that the Ensemble Kaman Filter (EnKF) algorithm using dynamic background error covariance is suitable for multi-variable data assimilation in polar regions because it does not need to develop complex adjoint models and is computationally efficient, and it has been widely used in Arctic sea ice forecasts (Sakov et al., 2012; Yang et al., 2014, 2015, 2016; Mu et al., 2018; Liang et al., 2019).

In order to address the pressing need for sea ice forecasts in the Southern Ocean, especially in support of Chinese National Antarctic Research Expedition (CHINARE), the motivation of this work is to describe a newly developed regional synoptic forecasting system for Antarctic sea ice, i.e., Southern Ocean Ice Prediction System version 1.0 (SOIPS V1.0), which is based on an sea-ice–ocean–ice-shelf coupled model and an EnKF data assimilation algorithm. The SOIPS operationally run since January 1, 2021, and provided sea ice forecasts for the 38th CHINARE-Antarctic during austral summer of 2021/2022. Here, by evaluating sea ice forecasts in a complete melt-freeze cycle between October 1, 2021 and September 30, 2022, we show in this study that this new system has a promise capacity of providing precise forecasts for Antarctic sea ice evolution at synoptic timescale, especially the forecast accuracy of sea ice drift is substantially guaranteed. The paper is organized as follows. In section 2, the system configuration and the data assimilation strategy are described in detail. Antarctic sea ice forecasts, including sea ice concentration, sea ice extent, sea ice thickness, sea ice drift and sea ice convergence rate, are evaluated in section 3. Conclusions and discussions are made in section 4.

2 System Description

2.1 Model Configuration

The regional sea-ice–ocean–ice-shelf coupled model of SOIPS is configured on the Massachusetts Institute of Technology general circulation model (MITgcm; Marshall et al., 1997; Losch et al., 2010). The ocean model uses curvilinear coordinates with the open boundaries far north away from the domain of the Antarctic Circumpolar Current (ACC). There are 496×496 grid points in horizontal with an average resolution of ~ 18 km (Fig. 1). Vertically, it is composed of 50 unevenly spaced layers with intervals from 10 m near the surface to 450 m at the bottom. The ocean model utilizing the finite-volume

https://doi.org/10.5194/gmd-2024-4
Preprint. Discussion started: 21 February 2024

Geoscientific Model Development Discussions

incompressible Navier-Stokes equations adopts the bulk formula at surface (Large and Pond, 1981) and the K-profile parameterization in the ocean interior (KPP; Large et al., 1994). The viscous-plastic rheology (Hibler, 1979; Zhang and Hibler, 1997) and the zero-layer ice/snow thermodynamics (Semtner, 1976) are used in the sea ice model, which shares the same horizontal mesh with the ocean model. The ice-shelf, serving as as a static surface boundary condition, exerts thermodynamic influence on the underlying ocean and thus affects ocean circulation and sea ice. Time step of the coupled model is 1200 seconds.

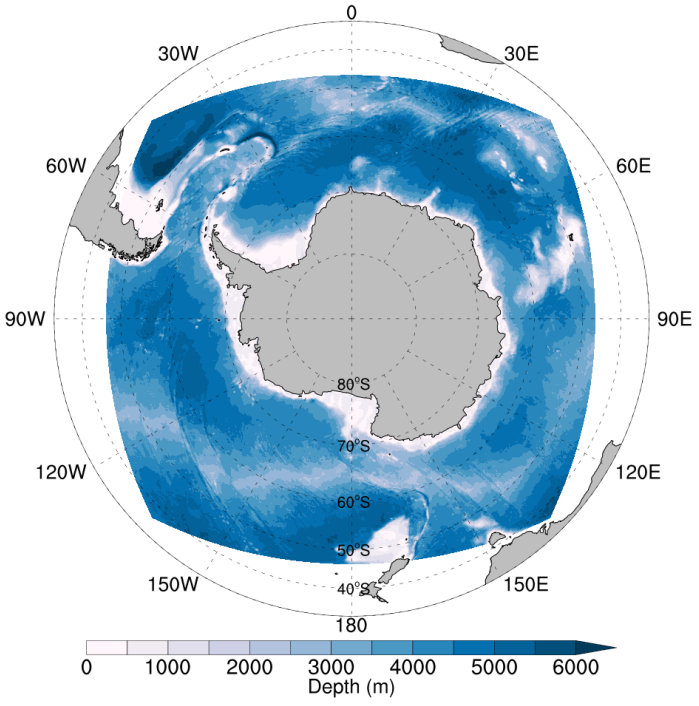

Figure 1: The domain of the Southern Ocean Ice Prediction System (SOIPS). The contours show the bathymetry in meters.

The initial fields of ocean temperature and salinity are derived from the World Ocean Atlas 2009 (WOA09; Locarnini et al., 2010; Antonov et al., 2010). The initial fields of sea ice concentration and thickness are obtained from observations of the Advanced Microwave Scanning Radiometer for the Earth Observing System (AMSR-E; Pedersen et al., 2017) and the Ice, Cloud, and land Elevation Satellite (ICESat; Zwally, 1990), respectively. The ice-shelf draft is obtained from a consistent data set of Antarctic ice sheet topography, cavity geometry, and global bathymetry (Timmermann et al. 2010). Climatological monthly mean oceanic boundary conditions are provided by the Estimating the Circulation and Climate of the Ocean phase II (ECCO2; Menemenlis et al., 2008), including ocean potential temperature, salinity, and velocity.

https://doi.org/10.5194/gmd-2024-4
Preprint. Discussion started: 21 February 2024

In our previous work, a model free run from 1979 to 2020 without data assimilation have been successfully conducted, which is forced by atmospheric variables at ocean surface derived from the Japanese 55-year Reanalysis (JRA55; Kobayashi et al., 2015; Harada et al., 2016) including 2-m air temperature and humidity, 10-m wind velocity components, downward shortwave and longwave radiation at the sea surface, and total precipitation. Validation of the model free run results including the simulated sea ice extent, sea ice concentration, sea ice thickness and net eastward oceanic volume transport across the Drake Passage has demonstrated that this regional sea-ice–ocean–ice-shelf coupled model is capable in capturing the main features of Antarctic sea ice and ocean (Zhao et al., 2023).

2.2 Data Assimilation Scheme

The data assimilation algorithm used in SOIPS is the ensemble-based Localized Error Subspace Transform Kalman Filter (LESTKF, Nerger et al., 2012), which is packaged in the Parallel Data Assimilation Framework (PDAF; Nerger and Hiller, 2013). LESTKF is a localized variant of the Error Subspace Transform Kalman Filter (ESTKF), in which the dynamic background error covariance is applied. An optimal localization scheme that allows for adaptive localization radius based on observation number is achieved by setting the effective local observation dimension equal to the ensemble size (Kirchgessner et al., 2014). Weights of observations within the optimal localization radius are calculated based on a 5-order polynomial function according to the distance between observation location and analysis grid point (Hunt et al., 2007; Gaspari and Cohn, 1999). Studies have indicated that LESTKF is suitable for high-dimensional models with small scale local features and large number of observations. Considering the balance between computational efficiency and forecasting skills, 12 ensemble members are selected for the SOIPS ensemble forecasts.

SOIPS start running operationally on January 1, 2021. The initial ensemble of SOIPS is generated by disturbing the latest state of the model free run. The 12 perturbations which are used to initialize the SOIPS ensemble are created by applying an order-2 sampling scheme to the leading 11 EOF modes of the daily model state evolution in the historical model free run between January 1, 2019 and December 31, 2020. During each assimilation step, near-real-time 6.25 km-resolution sea ice concentration data retrieved from the Advanced Microwave Scanning Radiometer 2 (AMSR2) brightness temperature data, are assimilated into the SOIPS and used to update sea ice concentration and thickness in the 12 ensemble initial fields on a daily basis. Since the uncertainties of the AMSR2 observations are not the same for different sea ice concentration ranges (Spreen et al., 2008), for simplicity a uniform value of 0.15 is assigned as the representative observation error. Specifically, a post-assimilation procedure is carried out that the modeled sea surface salinity is adjusted according to the formula described by Liang et al. (2019) to match with the change of sea ice thickness. Atmospheric forcing for operational forecasts are taken from the National Centers for Environmental Prediction (NCEP) Global Forecast System (GFS) 168-hour atmospheric forecasts. During each forecasting step, the 12 ensemble members after assimilating observed sea ice concentration are separately integrated for 168 hours, to create 12 members of 7-day forecasts and their ensemble mean is saved. The

https://doi.org/10.5194/gmd-2024-4
Preprint. Discussion started: 21 February 2024

Geoscientific Model Development Discussions

ensemble fields of the 24 h forecasts are also recorded as initial fields for the operational forecasts on the following day (Fig. 2).

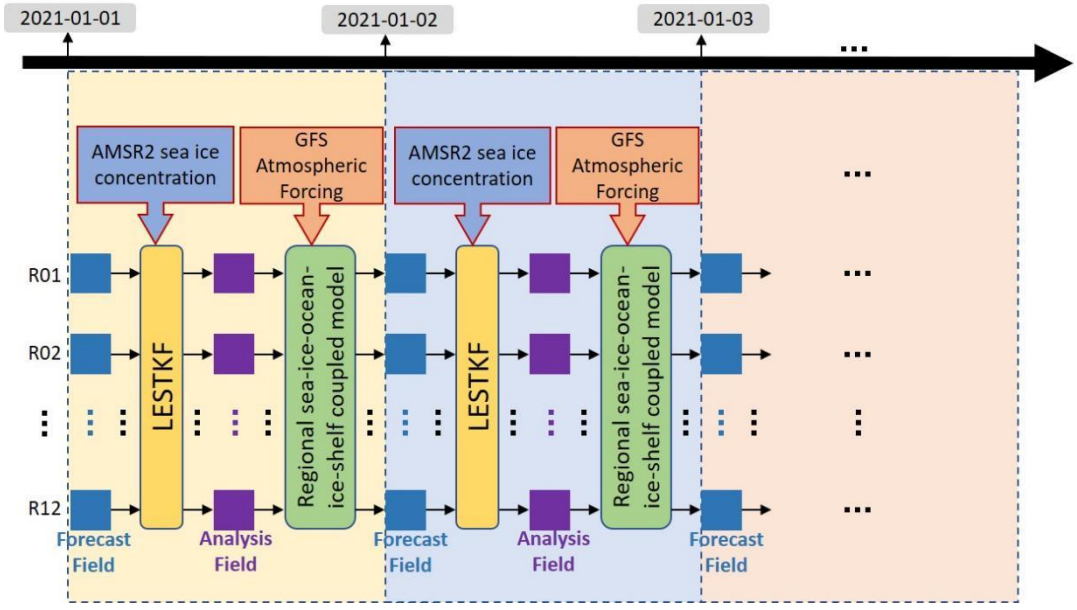

145 **Figure 2: Schematic diagram of the SOIPS. The blue and purple squares denote the 12 ensemble members of model state pre- and post- data assimilation step. The yellow block denotes the data assimilation model utilizing the ensemble-based LESTKF. The green block denotes the Antarctic regional sea-ice–ocean–ice-shelf coupled model. The blue block with thick arrow denotes the near-real-time AMSR2 sea ice concentration observation. The orange block with thick arrow denotes the operational GFS atmospheric forcing.**

150 ## 3 Evaluation of Sea Ice Forecasts

SOIPS had provided forecasts of sea ice concentration, sea ice thickness, sea ice drift, sea ice convergence rate for the 38th CHINARE-Antarctic during the austral summer of 2021/2022. Here, we evaluate the forecasting data during a complete melt-freeze cycle from October 1, 2021 to September 30, 2022.

3.1 Sea Ice Concentration

155 The sea ice concentration product of the EUMETSAT Ocean and Sea Ice Satellite Application Facility (OSISAF), delivered daily at 10km resolution in a polar stereographic projection, is used as an independent observation to evaluate the sea ice concentration forecasts. This product is computed from atmosphere-corrected brightness temperatures of the Special Sensor Microwave Imager/Sounder (SSMIS), using a combination of state-of-the-art algorithms which is different from the ASI algorithm used for AMSR2 sea ice concentration.

https://doi.org/10.5194/gmd-2024-4
Preprint. Discussion started: 21 February 2024

Geoscientific Model Development Discussions

We calculate root mean square errors (RMSEs) between the SOIPS forecasts at different leading time and the OSISAF sea ice concentration observations, to evaluate the performance of SOIPS on sea ice concentration forecasts (Fig. 3). As the spatial resolution of SOIPS is coarser than that of the OSISAF data, we interpolate the OSISAF data onto the model grid of SOIPS. Basically the RMSEs between the SOIPS forecasts and OSISAF data gradually increase in the melting season (October–February, hereafter the latter month in such expressions that the latter month is earlier than the former month denotes the month of the next year) and decrease in the freezing season (March–September). The RMSEs are generally lower than 0.15 during June–September while close to 0.2 during January–February. The evolution of the RMSEs has two peaks, one in December and the other in April. The maximum RMSE in April is lower than 0.33. Comparison of the SOIPS forecasts at different leading time shows that the RMSEs increase generally along with the prolong of forecast leading time. Statistical analysis reveals that annual mean RMSEs of sea ice concentration forecasts at leading times of 24-hour, 72-hour, 120-hour and 168-hour are 0.15, 0.16, 0.17 and 0.19, respectively. We also assess the difference between the assimilated AMSR2 sea ice concentration and the OSISAF data. Due to different remote sensors and retrieval algorithms, there are significant systematic deviations between the OSISAF and AMSR2 products. The RMSEs of these two products increase in the melting season reaching a maximum value of 0.24 in February, thereafter the RMSEs decrease rapidly in April maintaining below 0.15 in the rest of the freezing season. The systematic bias between the assimilated data and the validation data partly explains the sea ice concentration forecasting errors.

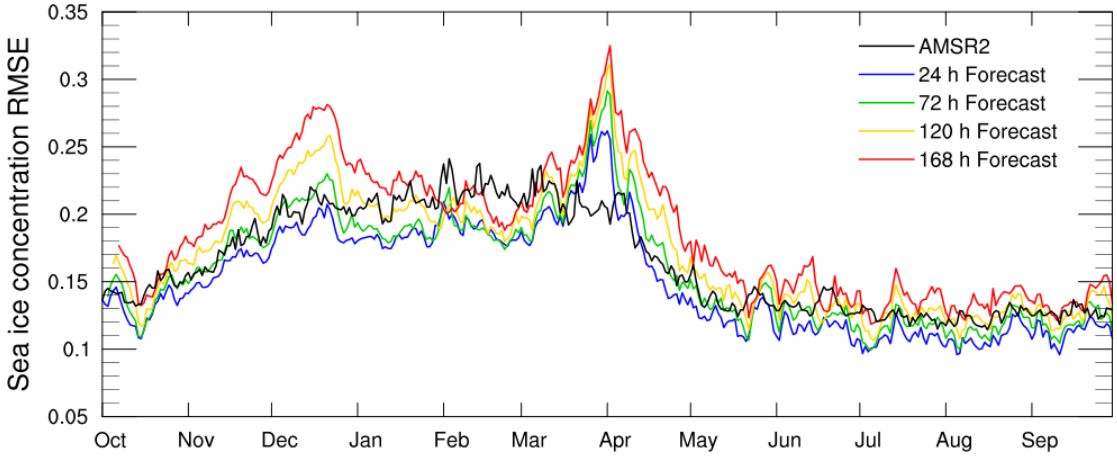

Figure 3: Time series of the RMSEs of the assimilated AMSR2 data and sea ice concentration forecasts at different leading time with respect to the OSISAF data. The blue, green, yellow, red, and black lines denote the sea ice concentration forecasts at leading time of 24-hour, 72-hour, 120-hour, 168-hour, and the AMSR2 data, respectively.

We further analyze spatial distribution of sea ice concentration forecasting errors by evaluating monthly mean fields of sea ice forecasts at leading time of 24-hour (Fig. 4). During October–November, relative large RMSEs of sea ice concentration forecasts mainly locate in the north marginal ice zone surrounding the Antarctica, where the sea ice, normally with relative low concentration and thickness, moves actively in response to external forces. In December, the RMSEs of sea ice

https://doi.org/10.5194/gmd-2024-4
Preprint. Discussion started: 21 February 2024

Geoscientific Model Development Discussions

185 concentration forecasts in the marginal ice zone greatly shrink except that in the Southern Atlantic Ocean sector between 30°W and 30°E. During January–February, the forecasting errors are small in entire ice zone except that in some nearshore areas of the eastern Antarctic. The forecasting errors start to increase in the Ross–Amundsen Seas along with the northward expansion of sea ice zone during March–April. In the following freezing months, relative large RMSEs of sea ice concentration forecasts reemerge in the north marginal ice zone but their amplitudes are lower than those in the previous
190 October–November.

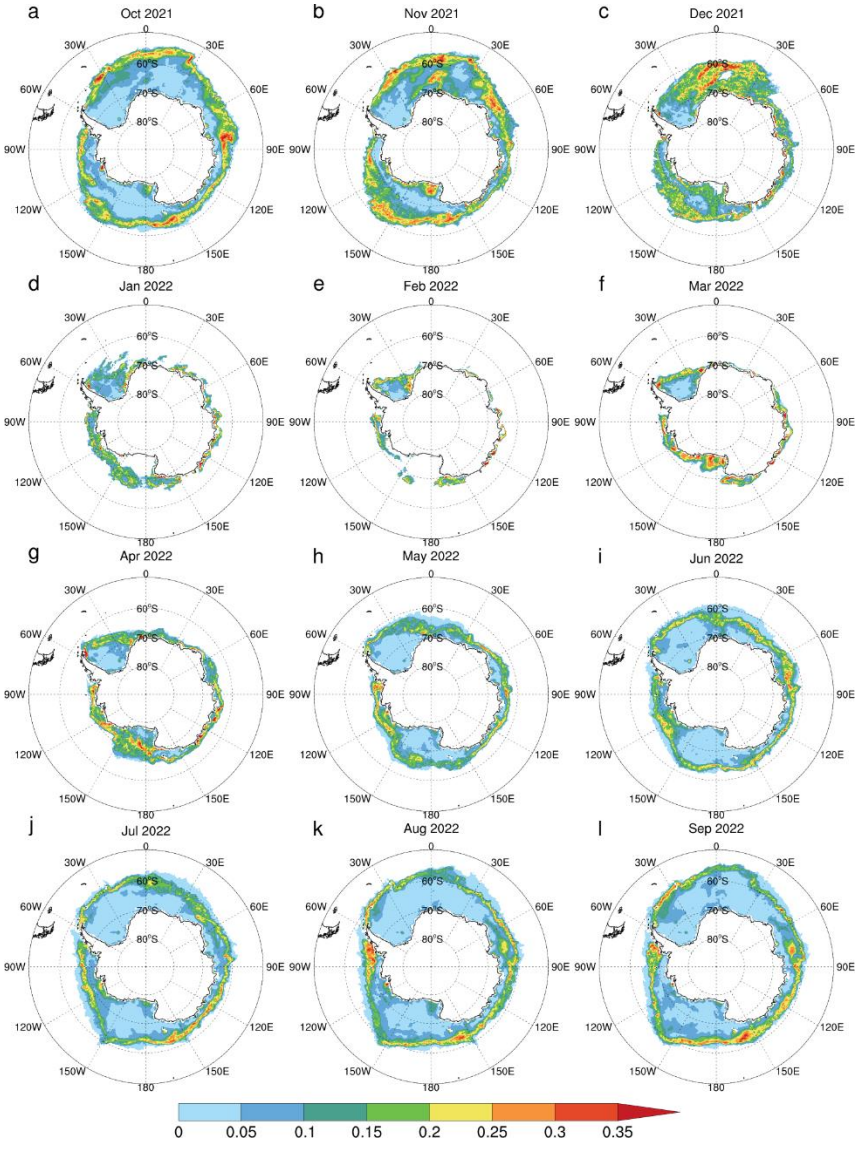

Figure 4: Monthly patterns of the RMSEs of sea ice concentration forecasts at leading time of 24-hour with respect to the OSISAF data. (a)–(l) denote October 2021–September 2022.

https://doi.org/10.5194/gmd-2024-4
Preprint. Discussion started: 21 February 2024

Geoscientific Model Development Discussions

3.2 Sea Ice Extent

Instead of evaluating just a number of sea ice extent, Goessling et al. (2016) has introduced a more useful verification metric, i.e. Integrated Ice-Edge Error (IIEE), which is the sum of all areas where the local sea ice extent is overestimated or underestimated. We use the sea ice edge (15% sea ice concentration) derived from the OSISAF data as a reference. First, we calculate the IIEEs between the assimilated AMSR2 and the OSISAF sea ice concentration data (Fig. 5). The IIEEs are larger than 0.5×10^6 km^2 during October–early January, and smaller than 0.5×10^6 km^2 in other months. The maximum IIEE occurs in December, with a value of 1.45×10^6 km^2. This systematic bias between the assimilated AMSR2 and the OSISAF data contributes to the first peak in the evolution of the RMSEs of sea ice concentration forecasts in December as shown in Figure 3.

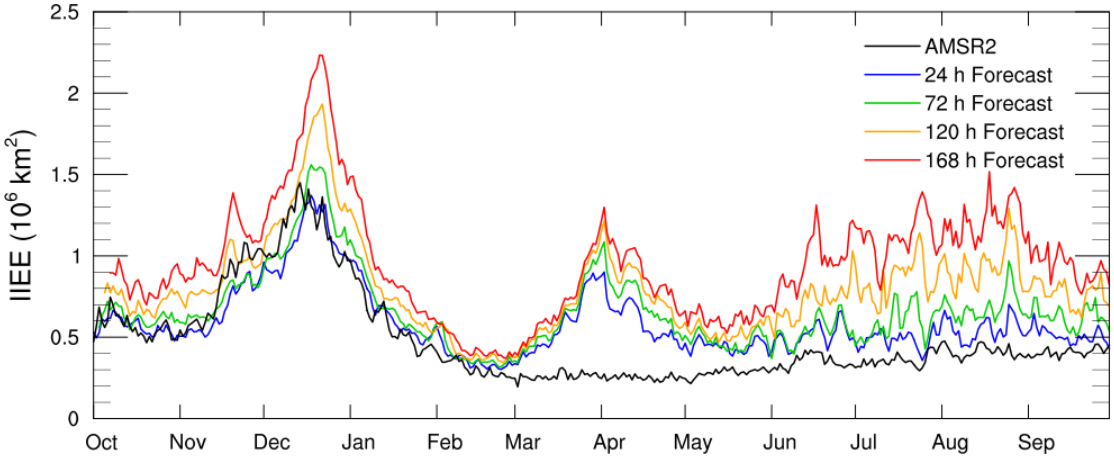

Figure 5: Time series of the IIEE forecasts at different leading time with respect to the OSISAF data. The blue, green, yellow, red, and black lines denote the IIEE forecasts at leading time of 24-hour, 72-hour, 120-hour, 168-hour, and the AMSR2 data, respectively.

Similarity the IIEEs between sea ice forecasts and the OSISAF data in the melting season follows that between the assimilated AMSR2 data and the OSISAF data. In December the maximum IIEEs of the forecasts at different leading time range from 1.35×10^6 km^2 to 2.25×10^6 km^2. In the early freezing season, large IIEEs of the forecasts reemerge at the end of March, corresponding to the second peak in the evolution of the RMSEs of sea ice concentration forecasts as shown in Figure 3. The large IIEEs in late March and early April can not be attributed to the systematic bias between the assimilated AMSR2 data and the OSISAF data, but rather the model ability in accurately simulating the expansion of sea ice cover in the early freezing season. During June–September, the IIEEs of sea ice forecasts at the leading time of 24-hour maintain around 0.5×10^6 km^2, and those of 72-hour maintain below 1×10^6 km^2.

Spatially at a first glance, the sea ice edge forecasts at leading time of 24-hour are generally coincident with those in the OSISAF data (Fig. 6). It is noteworthy that besides the contributor to the IIEEs from the north marginal ice zone, significant contributor to the IIEEs is from the nearshore areas surrounding the Antarctica in all the months. By carefully checking the

https://doi.org/10.5194/gmd-2024-4
Preprint. Discussion started: 21 February 2024

Geoscientific Model Development Discussions

coastlines or ice-shelf fronts of the Antarctica in the model domain and the OSISAF data, we realize that part of mismatch of sea ice edges in the nearshore areas is mendacious originating from the divergence of coastlines or ice-shelf fronts in the model domain and the OSISAF data. The real IIEEs between sea ice forecasts and the OSISAF data should be lower than those in Figure 5.

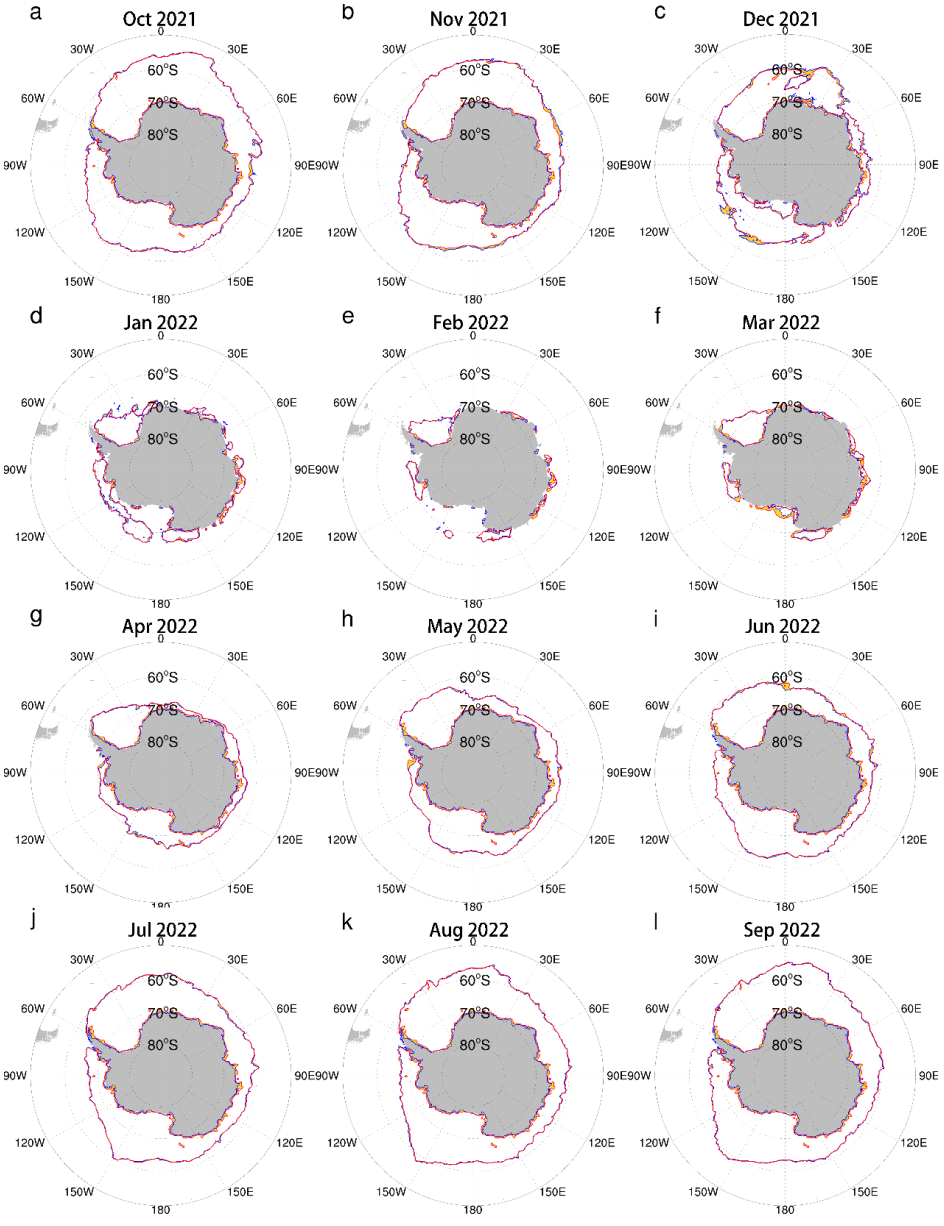

Figure 6: Monthly patterns of sea ice edge forecasts at leading time of 24-hour with respect to the OSISAF data. (a)-(l) denote October 2021–September 2022. The blue lines denote the SOIPS forecasts. The red lines denote the OSISAF data. The gold contours denote the IIEE.

https://doi.org/10.5194/gmd-2024-4
Preprint. Discussion started: 21 February 2024

Geoscientific Model Development Discussions

3.3 Sea Ice Thickness

At present, continuous observations of Antarctic sea ice thickness over large area are still difficult to obtain. With the launch of Ice, Cloud and Land Elevation Satellite-2 (ICESat-2) on September 15, 2018, the Antarctic sea ice freeboard can be estimated from measurements of the Advanced Topographic Laser Altimeter System (ATLAS) instrument. By applying the improved One-Layer Method (OLMi, Xu et al., 2021) to the daily gridded sea ice freeboard estimate product ATLAS/ICESat-2 L3B, we obtain daily Antarctic sea ice thickness distribution at discrete locations from October 1, 2021 to September 30, 2022.

Since the daily Antarctic sea ice thickness observations are available at discrete locations, we validate the daily evolution of the mean sea ice thickness forecasts at the discrete locations where observations on the corresponding date are available (Fig. 7). The results show that sea ice thickness forecasts at leading time of 24-hour are consistent with the ICESat-2 observations basically, but with an overestimation of sea ice thickness during October–November. In most time of the validation period, the mean absolute errors (MAEs) of the sea ice thickness forecasts at leading time of 24-hour are lower than 0.3 m, which is significantly smaller than the uncertainties of the ICESat-2 observations.

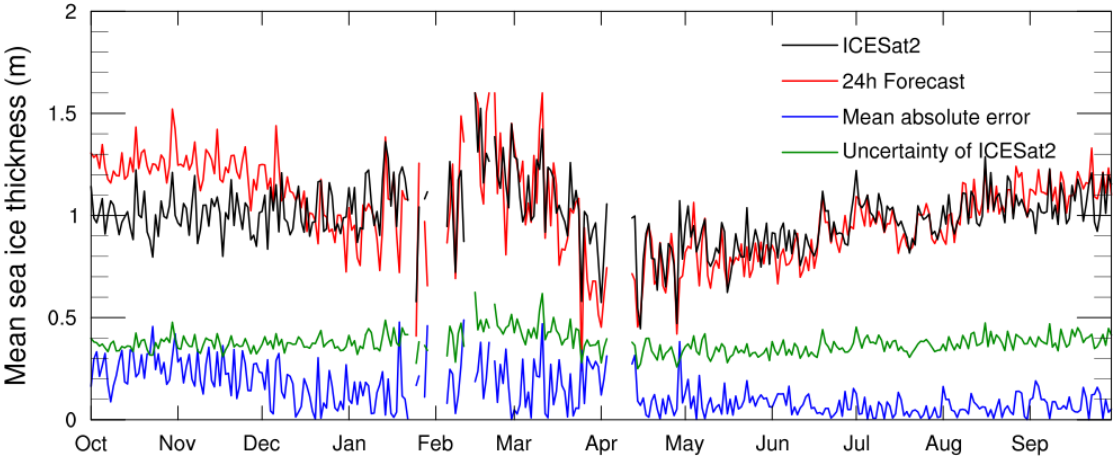

Figure 7: Time series of the mean ICESat-2 sea ice thickness observations (black lines), the sea ice thickness forecasts at leading time of 24-hour (red lines), the mean absolute errors between the ICESat2 data and sea ice thickness forecasts (blue lines), and the uncertainties of the ICESat2 sea ice thickness observations (green lines).

Now we merge the daily sea ice thickness observations into seasonal mean fields, and further evaluate spatial pattern of sea ice thickness forecasts at leading time of 24-hour (Fig. 8). The sea ice thickness forecasts show a good agreement with the observations, featured by thick ice locating in the Weddell Sea, the Amundsen Sea and the nearshore areas of the eastern Antarctic. During January–March, the SOIPS forecasts overestimate ice thickness in the southern Weddell Sea while underestimate ice thickness in the eastern Amundsen Sea. In other seasons, the SOIPS forecasts overestimate ice thickness in

https://doi.org/10.5194/gmd-2024-4
Preprint. Discussion started: 21 February 2024

Geoscientific Model Development Discussions

the western Ross Sea and the southern Weddell Sea, while underestimate ice thickness in the Amundsen Sea and the nearshore areas of the eastern Antarctic. Admittedly, the above evaluation ignores the errors caused by the spatiotemporal discontinuity and the uncertainties of the ICESat-2 observations.

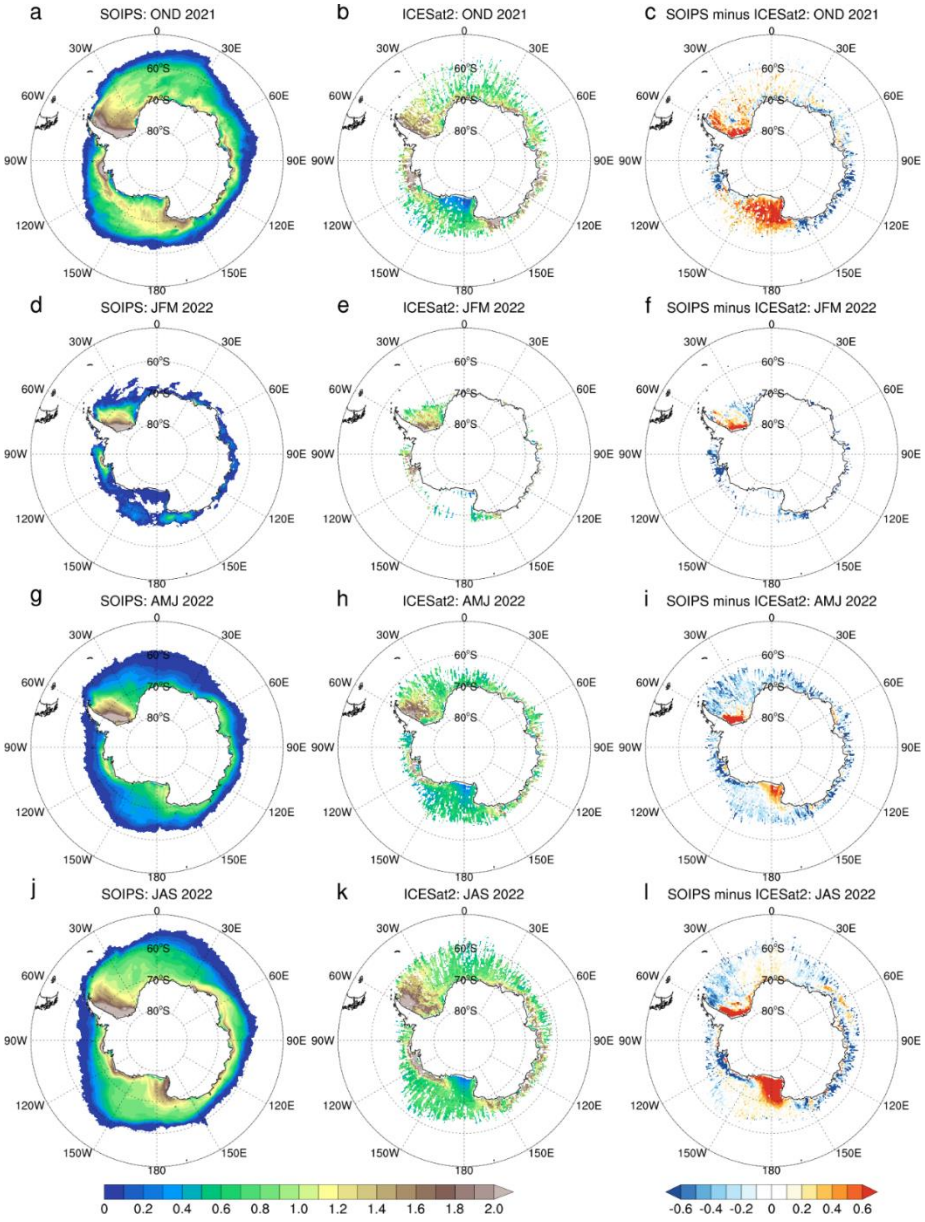

255 **Figure 8: Seasonal patterns of the Antarctic sea ice thickness. The left, middle, and right columns denote the SOIPS forecasts at leading time of 24-hour, the ICESat2 observations, and their deviations, respectively. The panels from top to bottom denote October–December, January–March, April–June, and July–September, respectively.**

https://doi.org/10.5194/gmd-2024-4
Preprint. Discussion started: 21 February 2024

Geoscientific Model Development Discussions

3.4 Sea Ice Drift

Polar pathfinder daily Antarctic sea ice motion product provided by the National Snow and Ice Data Center (NSIDC, Tschudi et al., 2019) is used to assess the Antarctic sea ice drift forecasts. This dataset is projected on the EASE grid with a spatial resolution of 25 km, including input data sources derived from the Advanced Very High Resolution Radiometer (AVHRR), AMSR-E, Scanning Multichannel Microwave Radiometer (SMMR), Special Sensor Microwave/Imager (SSM/I), and SSMIS sensors, the International Arctic Buoy Programme (IABP) buoys, and the National Centers for Environmental Prediction/National Center for Atmospheric Research (NCEP/NCAR) Reanalysis.

To validate sea ice drift forecasts, we first convert the NSIDC ice drift components (u_o, v_o) on the EASE coordinates into the ice drift components (u_m, v_m) on the model coordinates, then the ice drift direction, expressed by the angle α with reference to location-dependent coordinate of um, is derived as the four quadrant arctangent of (u_m, v_m). Note that α ranges between -180° and 180°. We can evaluate the bias of direction in the sea ice drift forecasts by assessing the deviation of α between the modeled and observed sea ice drift. The ice drift magnitude is independent of selected coordinates.

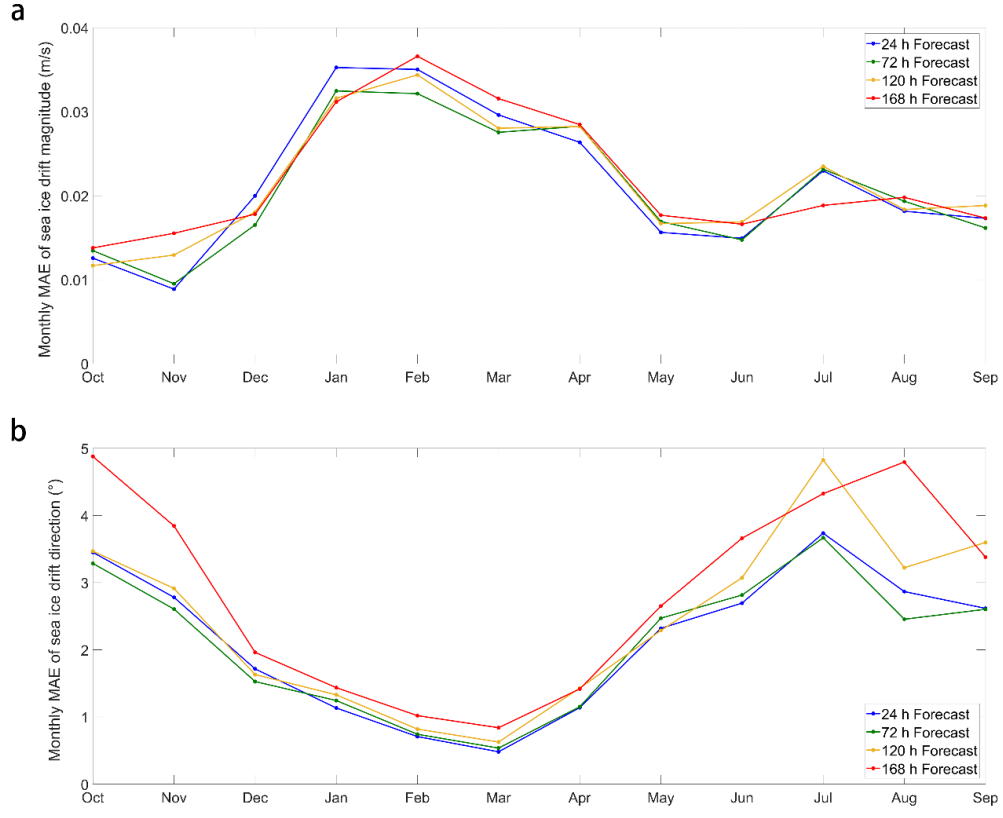

Figure 9: Time series of the monthly-mean MAEs of (a) magnitude and (b) direction of the sea ice drift forecasts at different leading time with respect to the NSIDC data. The blue, green, yellow, and red lines denote the sea ice drift forecasts at leading time of 24-hour, 72-hour, 120-hour, and 168-hour, respectively.

https://doi.org/10.5194/gmd-2024-4
Preprint. Discussion started: 21 February 2024

Validation results (Fig. 9) show that the MAEs of magnitude of sea ice drift between the SOIPS forecasts and observations increase during November–February and decrease during March–May. In contrary, the MAEs of direction of sea ice drift between the forecasts and observations decrease during October–February and increase during March–August. Along with the prolong of the forecast leading time, the MAEs of both magnitude and direction of the sea ice drift forecasts do not exhibit significant amplification. Statistical analysis (Table 1) shows that the annual mean magnitude of sea ice drift forecasting errors at leading time of 24-hour, 72-hour, 120-hour, and 168-hour are 2.14 cm/s, 2.09 cm/s, 2.17 cm/s, and 2.22 cm/s, respectively. As a reference, the derived magnitude of the NSIDC ice drift product are 10.22 cm/s during October–December, 4.78 cm/s during January–March, 10.55 cm/s during April–June, and 13.26 cm/s during July–September. The annual mean magnitude of sea ice drift forecasting errors at leading time of 168-hour accounts for 23% of the observed magnitude. It is noteworthy that the MAEs of magnitude of sea ice drift forecasts are relative higher during January–March in comparison with those in other seasons. The annual mean direction of sea ice drift forecasting errors at leading time of 24-hour, 72-hour, 120-hour, and 168-hour are 2.13°, 2.08°, 2.42°, and 2.81°, respectively. This results suggest that the SOIPS has a reliable performance on forecasting sea ice drift direction, although with a systematic positive bias in the magnitude of sea ice drift forecasts. Previous study conducted for the Arctic region has also found that the numerical overestimation of sea ice drift speed is a common feature in the CMIP6 models (Wang et al., 2023).

		Leading time of forecasts			
		24h	72h	120h	168h
MAEs of magnitude of sea ice drift (cm/s)	OND	1.42	1.35	1.45	1.61
	JFM	3.36	3.09	3.17	3.29
	AMJ	1.86	1.97	2.02	2.10
	JAS	1.95	1.95	2.02	1.86
	Average	2.14	2.09	2.17	2.22
MAEs of direction of sea ice drift (°)	OND	2.59	2.40	2.57	3.38
	JFM	0.79	0.85	0.93	1.11
	AMJ	2.06	2.15	2.28	2.58
	JAS	3.07	2.91	3.89	4.16
	Average	2.13	2.08	2.42	2.81

Table 1. The seasonal-mean MAEs of magnitude and direction of the sea ice drift forecasts at different leading time with respect to the NSIDC data.

3.5 Sea Ice Convergence Rate

Sea ice convergence rate is a useful metric in guiding ship navigation in sea ice zone. Sea ice disperses when the convergence rate is negative, and accumulates when the convergence rate is positive. The Antarctic China Zhongshan Station locates at (69°22'24.76"S, 76°22'14.28"E) in the Prydz Bay (Fig. 10). In the southern Prydz Bay there is a large area of landfast ice. Floating sea ice occupies the area north of the landfast ice zone. Under the forces of wind and tide, the

https://doi.org/10.5194/gmd-2024-4
Preprint. Discussion started: 21 February 2024

Geoscientific Model Development Discussions

floating sea ice zone sometimes adhere to the landfast ice zone closely, sometime keep away from the landfast ice zone creating an open water band between them.

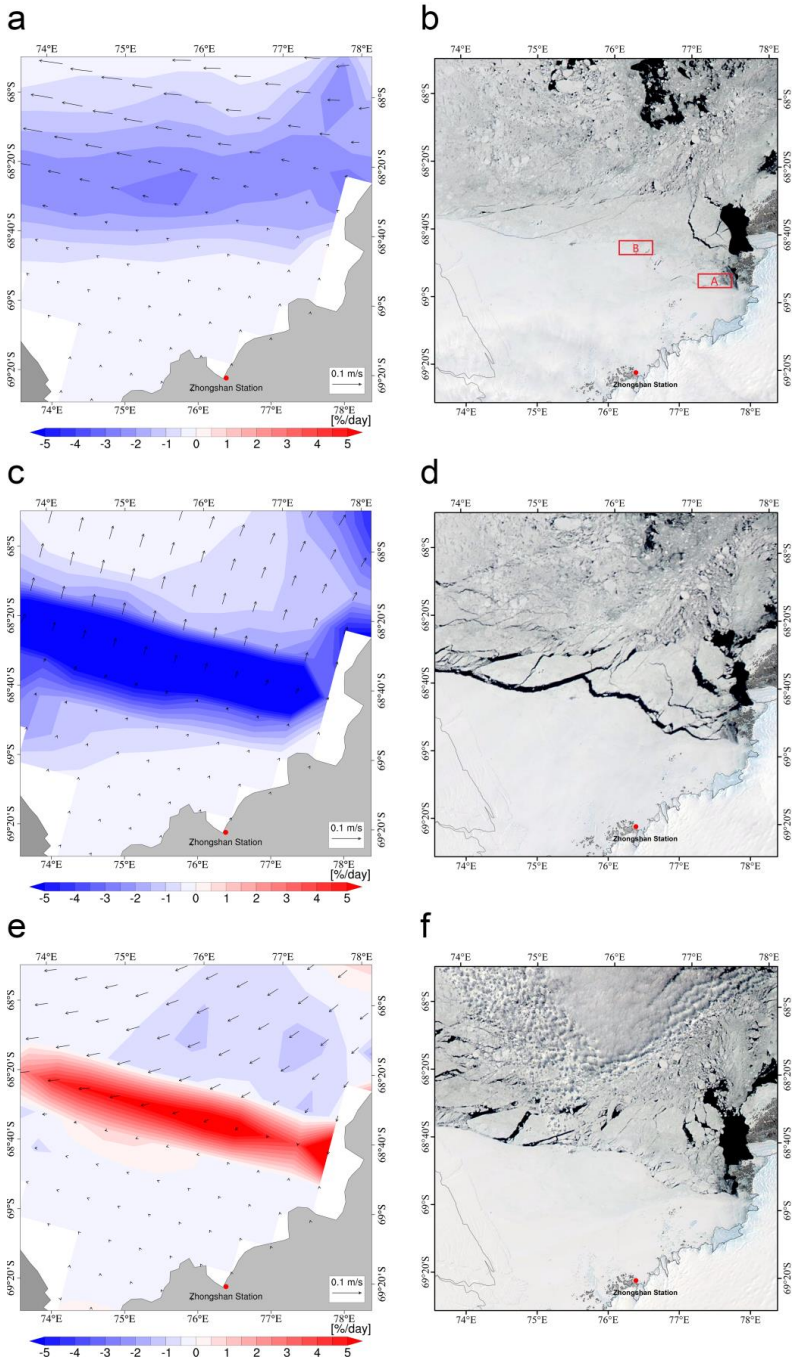

Figure 10: The SOIPS forecasts for sea ice convergence rate (left column) and the MODIS satellite images (right column). The top, middle, and bottom panels denote forecasts/observations on 2021 November 19, 20, and 21 respectively. Black arrows in the left

https://doi.org/10.5194/gmd-2024-4
Preprint. Discussion started: 21 February 2024


Geoscientific Model Development Discussions

column denote sea ice drift vectors, while red and blue contours indicate that sea ice drift in the corresponding area tends to convergent and divergent, respectively. The red dot in each figure marks the Antarctic China Zhongshan Station. The two boxes in (b) denotes two areas where the icebreaker *MV Xue Long* has arrived in some years.

The Chinese icebreaker *MV Xue Long* navigated to the Antarctic China Zhongshan Station to unload supplies almost every year in the past four decades. In some years, the icebreaker navigated southward to arrive the area of A through the relative loose floating sea ice zone in the eastern Prydz Bay. However, owing to the indurative ice condition with many ice ridges and neaped icebergs in the landfast ice zone south of the area of A, the icebreaker had to navigate to the area of B and then turned southward heading to the Antarctic China Zhongshan Station. The landfast ice condition in the areas south of the area of B is much friendly to the icebreaker. As a consequence, the timing of open water band between the floating sea ice zone and the landfast ice zone plays a crucial role in the icebreaker navigation from A to B.

Here we show a typical situation of how the sea ice convergence rate benefits for the navigation from A to B. Forecasting initialized on November 18, 2021, the SOIPS forecasts at leading time of 24-hour, 48-hour, and 72-hour suggested a weak negative ice convergence rate on November 19, 2021, a strong negative ice convergence rate on November 20, 2021, and a strong positive ice convergence rate on November 21, 2021. The ice convergence rate forecasts indicated the open water band between the floating sea ice zone and the landfast ice zone may occur on November 19, 2021, very likely to occur on November 20, 2021, and may disappear on November 21, 2021. The NASA MODIS images in the three days clearly validate the usability of the sea ice convergence rate forecasts during this opening-closing process of open water band.

4 Conclusion and Discussion

In this work we introduce an operational synoptic-scale sea ice forecasting system for the Southern Ocean, i.e. Southern Ocean Ice Prediction System (SOIPS). The system is developed to meet the increasing demands for synoptic-scale Antarctic sea ice forecasts at present and in the coming decade. The system is configured on an Antarctic regional sea-ice–ocean–ice-shelf coupled model and an ensemble-based LESTKF data assimilation model, and driven by operational atmospheric forecasting variables at ocean surface from international weather forecasting products. Near-real-time satellite sea ice concentration observations are assimilated into the system on a daily basis to update sea ice concentration and thickness in the 12 ensemble members of model state. The SOIPS forecasts has been engaged in sea ice service for the 38th Chinese National Antarctic Research Expedition for the first time.

By evaluating sea ice forecasts in a complete melt-freeze cycle between October 1, 2021 and September 30, 2022, this study find that the SOIPS has a reliable ability to forecast sea ice evolution on synoptic-scale. With respect to the OSISAF data, the RMSEs of sea ice concentration forecasts at leading time of up to 168-hour are generally lower than 0.15 during June–September while close to 0.2 during January–February, and the annual mean RMSEs are lower than 0.19. Relative large RMSEs of sea ice concentration forecasts mainly locate in the north marginal ice zone surrounding the Antarctica. The IIEEs

https://doi.org/10.5194/gmd-2024-4
Preprint. Discussion started: 21 February 2024


Geoscientific Model Development Discussions

of sea ice forecasts in most freezing months at leading times of 24-hour and 72-hour maintain around 0.5×10^6 km^2 and below 1.0×10^6 km^2, respectively. It should be mentioned that mismatch of sea ice edges in some nearshore areas originates from the divergence of coastlines or ice-shelf fronts in the model domain and the OSISAF data. The MAEs between sea ice thickness forecasts at leading time of 24-hour and the ICESat-2 observations are lower than 0.3 m, which is in range of the ICESat-2 uncertainties. The SOIPS also performs well on sea ice drift forecasts, both in magnitude and direction. Statistical analysis suggests that annual mean biases of sea ice drift forecasting errors at leading time of 168-hour with respect to the NSIDC sea ice motion data are 2.22 cm/s in magnitude and 2.81° in direction. Furthermore, sea ice convergence rate, which can be derived from sea ice velocity forecasts, has a high potential in supporting ship navigation on local fine scale. A typical application of how sea ice convergence rate forecasts benefit for the icebreaker navigation in the Prydz Bay is illustrated.

Satellite observations on sea ice concentration, thickness and drift have relative larger biases and scarcer coverage in the Antarctic in comparison with the Arctic, thus the evaluation of the SOIPS sea ice forecasts in this work still has considerable uncertainties. Part of the evaluation uncertainties come from the observational uncertainties themself, and part from the differences in spatialtemporal resolutions, as well as the coastline sharp, between the SOIPS and the observations. Accurate short-term sea ice forecasts rely on optimized initial conditions at the forecasting onset, precise atmospheric forcing data if using an ice-ocean coupled model, and the model physics in representing sea ice melt-freeze process and its heat and momentum exchanges with the underlying ocean. Specifically, the complex interactions among atmosphere, sea ice, ocean, ice-shelf, ice-sheet in the Antarctic region make the Antarctic sea ice forecasts more difficult. Moreover, in the Antarctic regional sea ice–ocean modeling, how to deal with oceanic open boundary conditions is a big challenge since the broad mid-latitude ocean surrounding the Antarctica can impact the Antarctic ocean and sea ice from all directions, i.e. Southern Pacific Ocean, Southern Atlantic Ocean, and Southern Indian Ocean. The utilizing of climatological monthly mean oceanic boundary conditions from the ECCO2 data makes the current configuration of the SOIPS lack of interannual variance at the model boundary originating from ocean variability in the lower latitudes. Although the Antarctic sea ice forecasts based on global models (Blockley et al., 2014; Posey et al., 2015; Smith et al., 2016; Lellouche et al., 2018; (Johnson et al., 2019) carried out by international weather forecasting centers avoid the problem of dealing oceanic boundary conditions, this newly developed regional sea ice forecasting system, as a new member of the international Antarctic sea ice forecasting system community, can operationally provide available sea ice forecasting information for the Southern Ocean at a moderate resolution and a higher computational efficiency.

We have successfully applied synchronized assimilation of the satellite-observed sea ice concentration, sea ice thickness, and sea surface temperature in our sea ice forecasting system for the Arctic, i.e. the Arctic Ice Ocean Prediction System (Mu et al., 2019; Liang et al., 2019). Owing to the rarity of operational satellite sea ice thickness observations with high spatial-temporal coverage in the Antarctic, the current version of the SOIPS only assimilates the AMSR2 sea ice concentration observations. In future, along with the elevation of satellite observation capacity, more and more sea ice and ocean variables are scheduled to be assimilated into the SOIPS to promote its ability on the Antarctic sea ice forecasts. Besides, more precise

https://doi.org/10.5194/gmd-2024-4
Preprint. Discussion started: 21 February 2024

atmospheric forcing data, more advanced model sea ice-ocean physics, and more satellite and in situ observations are urgently needed to support the numerical sea ice forecasts for the Southern Ocean.

Code and data availability. The MODIS images is accessed at https://worldview.earthdata.nasa.gov; The WOA09 data is accessed at https://www.nodc.noaa.gov/OC5/WOA09; The GFS data is accessed at https://www.ncei.noaa.gov/products/weather-climate-models/global-forecast; The AMSR-E data is accessed at https://nsidc.org/data/AU_SI25/versions/1; The ICESat data is accessed at https://nsidc.org/data/nsidc-0304; The ATLAS/ICESat-2 L3B data is accessed at https://nsidc.org/data/atl20/versions/4; The Polar Pathfinder data is accessed at https://nsidc.org/data/nsidc-0116/versions/4; The JRA-55 data is accessed at http://jra.kishou.go.jp/JRA-55; The AMSR2 data is accessed at https://seaice.uni-bremen.de/sea-ice-concentration; The OSISAF data is accessed at http://osisaf.met.no/p/ice; The PDAF software is accessed at https://pdaf.awi.de/trac/wiki; The SOIPS used to produce the results in this paper can be accessed at https://doi.org/10.5281/zenodo.10457661.

Author contributions. F. Zhao conducted the SOIPS and data analysis, and composed the initial draft. X. Liang revised the initial draft. Z. Tian, M. Li, N. Liu and C. Liu contributed to data analysis and revising the initial draft.

Competing interests. The authors declare that they have no conflict of interest.

Acknowledgments. The authors sincerely thank the NASA for the MODIS images; the NCEP for the WOA09 data and the GFS data; the NSIDC for the AMSR-E ice concentration data, the ICESat ice thickness data, the ATLAS/ICESat-2 L3B ice freeboard data, and the Polar Pathfinder ice motion data; the Japanese Meteorological Agency for the JRA55 data; the University of Bremen for the AMSR2 ice concentration data; the Norwegian Meteorological Institute for the OSISAF ice concentration data. We also acknowledge the developer of the PDAF software.

Financial support. This work is supported by the National Key R&D Program of China (2022YFF0802000) and the National Natural Science Foundation of China (42276250).

References

Antonov, J. I., Seidov, D., Boyer, T. P., Locarnini, R. A., Mishonov, A. V., Garcia, H. E.: World Ocean Atlas 2009, Volume 2: Salinity, NOAA Atlas NESDIS 69, NOAA, U.S. Government Printing Office,Washington D.C., 2010.

https://doi.org/10.5194/gmd-2024-4
Preprint. Discussion started: 21 February 2024


Geoscientific Model Development Discussions

Blockley, E. W., Martin, M. J., McLaren, A. J., and Coauthors: Recent development of the Met Office operational ocean forecasting system: an overview and assessment of the new Global FOAM forecasts, Geosci. Model Dev., 7, 2613–2638, 2014.

Cummings, J. A., and Smedstad, O. M.: Ocean data impacts in global HYCOM, J. Atmos. Ocean. Tech., 31(8), 1771-1791, 2014.

Gaspari, G. and Cohn, S. E.: Construction of correlation functions in two and three dimensions, Q. J. Roy. Meteor. Soc. 125, 723–757, 1999.

Goessling, H. F., Tietsche, S., Day, J. J., Hawkins, E., and Jung, T.: Predictability of the Arctic sea ice edge, Geophys. Res. Lett. 43, 1642–1650, 2016.

Harada, Y., Kamahori, H., Kobayashi, C., and Coauthors: The JRA-55 reanalysis: Representation of atmospheric circulation and climate variability, J. Meteorol. Soc. Jpn. Ser. II, 94, 269–302, 2016.

Heil, P. and Allison, I.: The pattern and variability of Antarctic sea-ice drift in the Indian Ocean and western Pacific sectors, J. Geophys. Res., 104 , 15789–15802, 1999.

Hibler III, W. D.: A dynamic thermodynamic sea ice model, J. Phys. Oceanogr., 9: 815–846, 1979.

Hunt, B. R., Kostelich, E. J., and Szunyogh, I.: Efficient data assimilation for spatiotemporal chaos: a local ensemble transform Kalman filter, Physica D, 230, 112–126, 2007.

Johnson, S. J., Stockdale, T. N., Ferranti, L., and Coauthors: SEAS5: the new ECMWF seasonal forecast system, Geosci. Model Dev., 12(3), 1087-1117, 2019.

Kirchgessner, P., Nerger, L., and Bunse-Gerstner, A.: On the choice of an optimal localization radius in ensemble Kalman filter methods, Mon. Weather Rev., 142(6), 2165-2175, 2014.

Kobayashi, S., Ota, Y., Harada, Y., and Coauthors: The JRA-55 reanalysis: general specifcations and basic characteristics, J. Meteorol. Soc. Jpn. Ser. II, 93(1):5–48, 2015.

Large, W. G. and Pond, S.: Open ocean momentum flux measurements in moderate to strong winds, J. Phys. Oceanogr., 11, 324-336, 1981.

Large, W. G., Mcwilliams, J. C., and Doney, S. C.: Oceanic vertical mixing: A review and a model with a nonlocal boundary layer parameterization, Rev. Geophys., 32, 363–403, 1994.

Lellouche, J. M., Greiner, E., Le Galloudec, O., and Coauthors: Recent updates to the Copernicus Marine Service global ocean monitoring and forecasting real-time 1/12∘ high-resolution system, Ocean Sci., 14(5), 1093-1126, 2018.

Liang, X., Losch, M., Nerger, L., Mu, L., Yang, Q., and Liu, C.: Using sea surface temperature observations to constrain upper ocean properties in an Arctic sea ice-ocean data assimilation system, J. Geophys. Res.-Oceans, 124(7), 4727-4743, 2019.

Liang, X., Zhao, F., Li, C., Zhang, L., and Li, B.: Evaluation of ArcIOPS sea ice forecasting products during the ninth CHINARE-Arctic in summer 2018, Adv. Polar Sci., 31(1), 14-25, 2020.

https://doi.org/10.5194/gmd-2024-4
Preprint. Discussion started: 21 February 2024


Geoscientific Model Development Discussions

Lindsay, R. W., and Zhang, J.: Assimilation of ice concentration in an ice–ocean model, J. Atmos. Ocean. Tech., 23(5), 742-749, 2006.

Locarnini, R. A., Mishonov, A. V., Antonov, J. I., Boyer, T. P., Garcia, H. E.: World Ocean Atlas 2009, Volume 1: Temperature, NOAA Atlas NESDIS 68, NOAA, U.S. Government Printing Office,Washington D.C., 2010.

Losch, M., Menemenlis, D., Campin, J. M., Heimbach, P., and Hill, C.: On the formulation of sea-ice models. Part 1: effects of different solver implementations and parameterizations, Ocean Model., 33(1-2), 129–144, 2010.

Luo, H., Yang, Q., Mu, L., and Coauthors: DASSO: a data assimilation system for the Southern Ocean that utilizes both sea-ice concentration and thickness observations, J. Glaciol., 67(266), 1235-1240, 2021.

Marshall, J., Adcroft, A., Hill, C., and Coauthors: A finite-volume, incompressible Navier Stokes model for studies of the ocean on parallel computers, J. Geophys. Res., 102(C3): 5753-5766, 1997.

Massonnet, F., Mathiot, P., Fichefet, T., and Coauthors: A model reconstruction of the Antarctic sea ice thickness and volume changes over 1980–2008 using data assimilation, Ocean Model., 64, 67-75, 2013.

Menemenlis, D., Campin, J. M., Heimbach, P., and Coauthors: ECCO2: High resolution global ocean and sea ice data synthesis, Mercator Ocean Quarterly Newsletter. 31:13–21, 2008.

Mignac, D., Martin, M., Fiedler, E., Blockley, E., and Fournier, N.: Improving the Met Office's Forecast Ocean Assimilation Model (FOAM) with the assimilation of satellite-derived sea-ice thickness data from CryoSat-2 and SMOS in the Arctic, Q. J. Roy. Meteor. Soc., 148(744), 1144-1167, 2022.

Mogensen, K., Balmaseda, M. A., and Weaver, A.: The NEMOVAR ocean data assimilation system as implemented in the ECMWF ocean analysis for System 4, ECMWF Tech. Memo., 668, 1-59, 2012.

Mogensen, K., Balmaseda, M. A., Weaver, A. T., Martin, M., and Vidard, A.: NEMOVAR: A variational data assimilation system for the NEMO ocean model, ECMWF newsletter, 120, 17-22, 2009.

Mu, L., Liang, X., Yang, Q., Liu, J., and Zheng, F.: Arctic Ice Ocean Prediction System: evaluating sea-ice forecasts during Xuelong's first trans-Arctic Passage in summer 2017, J. Glaciol., 65(253), 813-821, 2019.

Mu, L., Yang, Q., Losch, M., Losa, S. N., Ricker, R., Nerger, L., and Liang, X.: Improving sea ice thickness estimates by assimilating CryoSat-2 and SMOS sea ice thickness data simultaneously, Q. J. Roy. Meteor. Soc., 144(711), 529-538, 2018.

Nerger, L., Hiller, W.: Software for ensemble-based data assimilation systems-implementation strategies and scalability, Comput. Geosci., 55, 110-118, 2013.

Nerger, L., Janji, T., Schröter, J., and Coauthors: A unification of ensemble square root Kalman filters, Mon. Weather Rev., 140(7), 2335-2345, 2012.

Pedersen, L. T., Dybkjaer, G., Eastwood, S., and Coauthors: ESA Sea Ice Climate Change Initiative (Sea_Ice_cci): Sea Ice Concentration Climate Data Record from the AMSR-E and AMSR-2 instruments at 25km grid spacing, version 2.1, 2017.

https://doi.org/10.5194/gmd-2024-4
Preprint. Discussion started: 21 February 2024


Geoscientific Model Development Discussions

Posey, P. G., Metzger, E. J., Wallcraft, A. J., and Coauthors: Assimilating high horizontal resolution sea ice concentration data into the US Navy's ice forecast systems: arctic Cap Nowcast/Forecast System (ACNFS) and the Global Ocean Forecast System (GOFS 3.1), Cryosphere, 9, 2339–2365, 2015.

Ren, S., Liang, X., Sun, Q., and Coauthors: A fully coupled Arctic sea-ice–ocean–atmosphere model (ArcIOAM v1. 0) based on C-Coupler2: model description and preliminary results, Geosci. Model Dev., 14(2), 1101-1124, 2021.

Sakov, P., Counillon, F., Bertino, L., Lisæter, K. A., Oke, P. R., and Korablev, A.: TOPAZ4: an ocean-sea ice data assimilation system for the North Atlantic and Arctic, Ocean Sci., 8(4), 633-656, 2012.

Semtner Jr, A. J.: A model for the thermodynamic growth of sea ice in numerical investigations of climate, J. Phys. Oceanogr., 6(3): 379-389, 1976.

Smith, G. C., Roy, F., Reszka, M., and Coauthors: Sea ice forecast verification in the Canadian global ice ocean prediction system, Q. J. Roy. Meteor. Soc., 142(695), 659-671, 2016.

Spreen, G., Kaleschke, L. and Heygster, G.: Sea ice remote sensing using AMSR-e 89-GHz channels, J. Geophys. Res.-Oceans, 113,C02S03, 2008.

Timmermann, R., Le Brocq, A., Deen, T., and Coauthors: A consistent data set of Antarctic ice sheet topography, cavity geometry, and global bathymetry, Earth Syst. Sci. Data, 2(2), 261–273, 2010.

Tranchant, B., Testut, C. E., Ferry, N., and Brasseur, P.: SAM2: The second generation of Mercator assimilation system, European Operational Oceanography: Present and Future, 650, 2006.

Tschudi, M., Meier, W. N., Stewart, J. S., Fowler, C., and Maslanik, J.: Polar Pathfinder Daily 25km EASE-Grid Sea Ice Motion Vectors, Version 4 [Indicate subset used], Boulder, Colorado USA.NASA National Snow and Ice Data Center Distributed Active Archive Center, 2019.

Turner, J., Harangozo, S. A., Marshall, G. J., King, J. C., and Colwell, S. R.: Anomalous atmospheric circulation over the Weddell Sea, Antarctica during the Austral summer of 2001/02 resulting in extreme sea ice conditions, Geophys. Res. Lett., 29(24), 13-1, 2002.

Turney, C.: This was no Antarctic pleasure cruise, Nature 505, 133, 2014.

Wagner, P. M., Hughes, N., Bourbonnais, P., and Coauthors: Sea-ice information and forecast needs for industry maritime stakeholders, Polar Geogr., 43, 160–187, 2020.

Wang, X., Lu, R., Wang, S., and Coauthors: Assessing CMIP6 simulations of Arctic sea ice drift: Role of near-surface wind and surface ocean current in model performance, Adv. Clim. Chang Res., 14(5), 691-690, 2023.

Wang, Z., Turner, J., Sun, B. and Coauthors: Cyclone-induced rapid creation of extreme Antarctic sea ice conditions, Sci. Rep., 4, 5317, 2014.

Witze, A.: Researchers question rescued polar expedition, Nature, 505(7483), 270-271, 2014.

Womack, A., Vichi, M., Alberello, A., and Toffoli, A.: Atmospheric drivers of a winter-to-spring Lagrangian sea-ice drift in the Eastern Antarctic marginal ice zone, J. Glaciol., 68(271), 999-1013, 2022.

https://doi.org/10.5194/gmd-2024-4
Preprint. Discussion started: 21 February 2024

Worby, A. P., Massom, R. A., Allison, I., Lytle, V. I., and Heil, P.: East Antarctic sea ice: A review of its structure, properties and drift, Antarctic sea ice: physical processes, interactions and variability, 74, 41-67, 1998.

Xu, Y., Li, H., Liu, B., Xie, H., and Ozsoy-Cicek, B.: Deriving Antarctic sea-ice thickness from satellite altimetry and estimating consistency for NASA's ICESat/ICESat-2 missions, Geophys. Res. Lett., 48(20), 2021.

Yang, Q., Losa, S. N., Losch, M., and Coauthors: Assimilating summer sea-ice concentration into a coupled ice–ocean model using a LSEIK filter, Ann. Glaciol., 56(69), 38-44, 2015.

Yang, Q., Losa, S. N., Losch, M., and Coauthors: Assimilating SMOS sea ice thickness into a coupled ice-ocean model using a local SEIK filter, J. Geophys. Res.-Oceans, 119, 6680–6692, 2014.

Yang, Q., Losch, M., Losa, S. N., Jung, T., Nerger, L., and Lavergne, T.: Brief communication: The challenge and benefit of using sea ice concentration satellite data products with uncertainty estimates in summer sea ice data assimilation, Cryosphere, 10(2), 761–774, 2016.

Zhai, M., Li, X., Hui, F., and Coauthors: Sea-ice conditions in the Adélie Depression, Antarctica, during besetment of the icebreaker RV Xuelong, Ann. Glaciol., 56(69), 160-166, 2015.

Zhang, J., Hibler III, W. D.: On an efficient numerical method for modeling sea ice dynamics, J. Geophys. Res., 102: 8691–8702, 1997.

Zhao, F., Liang, X., Tian, Z., Liu, C., and Coauthors: Impacts of the long-term atmospheric trend on the seasonality of Antarctic sea ice, Clim. Dynam., 60(5-6), 1865-1883, 2023.

Zwally, H. J., Brenner, A. C., Major, J. A. and Bindschadler, R. A.: Satellite radar altimetry over ice, NASA Ref. Pub. 1233, vol. 1, section 5.0, 47–54, 1990.